Palestine Journal of Mathematics

Vol 15(2)(2026) , 616–634

Dynamic Behavior of Two Riccati Feedback Control Problems Generated by Distributed Delay Differential Equations

A.M.A. El-Sayed, S.M. Salman and M.A. Saad

Communicated by: Fathalla Ali Rihan

MSC 2020 Classifications: 37Mxx, 34Dxx , 37Gxx, 34Cxx .

Keywords and phrases: Riccati, Stability, Distributed Delay, Bifurcation, Chaos control.

The authors would like to thank the reviewers and editor for their constructive comments and valuable suggestions that improved the quality of our paper

Corresponding Author: M.A. Saad

Abstract. This paper presents a comprehensive analysis of the stability characteristics of Riccati differential equations in both discrete- and continuous-time frameworks, with particular emphasis on the impact of varying system parameters. An in-depth stability investigation examines the role of the parameter α in distributed-delay systems and its influence on overall system behavior. Two distinct Riccati models are compared, and their respective stability regions are identified while exploring the effects of parameter variations. Furthermore, the system dynamics are analyzed through the computation of the maximal Lyapunov exponent and phase portraits, which reveal transitions from stable to chaotic regimes. To enhance stability, a chaos control method is applied, effectively stabilizing the system within chaotic regions. The findings highlight the critical role of α in regulating system stability and provide valuable insights into the dynamic response of Riccati systems under parameter variations.

1 Introduction

Understanding differential equations is essential for grasping the behavior of dynamic systems across various scientific disciplines. **Delay differential equations (DDEs)**, a specialized class of differential equations, incorporate past states to predict current behavior, making them particularly valuable for modeling systems with inherent delays. The exploration of delay equations dates back to Wiener's foundational work on functional differential equations in the 1940s [1]. Since then, DDEs have been widely applied in biology, chemistry, physics, engineering, and economics to capture memory-dependent phenomena.

In **biological systems**, DDEs model population and disease dynamics, where growth or infection rates depend on previous states. For example, Banerjee et al. [2] demonstrated how time delays induce oscillations and chaotic behavior in predator–prey systems, while Bajiya et al. [3] extended this to epidemic models, showing that immune response delays significantly affect disease transmission and stability. These studies collectively highlight how delays can serve as a mechanism for both stabilizing and destabilizing biological processes.

In **chemical and physical systems**, DDEs have been used to analyze oscillatory reactions and optical feedback systems. Torbensen et al. [4] modeled the Belousov–Zhabotinsky reaction to show that delayed feedback can produce complex oscillatory and chaotic patterns. Similarly, Chembo et al. [5] and Larger et al. [6] investigated optical resonators and lasers, where delay-induced feedback leads to bistability and chaos. Collectively, these works bridge the gap between natural oscillatory mechanisms and engineered feedback systems.

In **engineering and control theory**, delays arise naturally due to finite signal transmission or feedback loops. Richard [7] analyzed such effects and developed stability criteria for delayed feedback systems, providing practical guidelines for controller design. In **economics**, Bianca et al. [8] and Bischi et al. [9] explored how past decisions or delayed reactions influence long-term

equilibrium and stability in macroeconomic and oligopolistic models.

The **concept of distributed delay** generalizes discrete delays by allowing the influence of past states to be spread continuously over time [10]. This idea has been widely used to describe systems with gradual memory fading, such as ecological and physiological processes. For instance, Zhang et al. [11] analyzed distributed delays in predator–prey systems, revealing that extended memory effects can generate sustained oscillations and complex dynamics. Likewise, Guerrini et al. [12] examined distributed delays in economic monopolies, showing that the shape of the delay kernel crucially determines system stability.

Recently, the incorporation of distributed and fractional delays has attracted growing attention for their ability to capture memory and hereditary effects in real-world systems. For instance, Rihan et al. [13] investigated a Caputo fractional-order asymptomatic COVID-19 model with multiple time delays, illustrating how fractional operators and delay interactions influence disease persistence and bifurcation behavior. Likewise, the fractional-order delay differential model of a tumor–immune system with vaccine efficacy proposed by Rihan et al. [14] revealed complex stability transitions and control mechanisms governed by delay parameters. Collectively, these studies highlight the increasing significance of integrating fractional calculus with delay structures to enhance the understanding of nonlinear biological and engineering systems.

In this context, the present study extends these ideas by analyzing a class of **distributed-delay Riccati-type differential equations**, where nonlinear integral memory terms govern system evolution. Two distinct formulations are compared to highlight how the placement of the nonlinear term within the integral affects the system's dynamic behavior. Through stability, bifurcation, and Lyapunov analyses, the results provide new insights into transitions from stable to chaotic regimes and illustrate how distributed delays can serve as a mechanism for controlling stability in both biological and feedback control models.

The delayed Riccati differential equation is given by [15, 16]

$$\frac{dx(t)}{dt} = 1 - \rho x^2(t-r). \tag{1.1}$$

Rather than focusing on the discrete delay in equation (1.1), we consider the following two types of distributed-delay Riccati differential equations (DD-RDEs):

$$\frac{dx(t)}{dt} = 1 - \rho \left[\int_0^t K(t-s)x(s)\,ds\right]^2, \tag{1.2}$$

and

$$\frac{dx(t)}{dt} = 1 - \rho \int_0^t K(t-s)x^2(s)\,ds, \tag{1.3}$$

where $\rho > 0$.

The two Riccati-type problems presented above involve distributed delays but differ fundamentally in how the delayed terms are incorporated. In the first equation (1.2), the delay term involves the square of the integral of past states $x(t)$ weighted by a kernel function $K(t)$. This formulation implies that the effects of past states are accumulated over time and then squared, potentially leading to a nonlinear amplification of past influences on the current state.

In contrast, the second equation (1.3) directly integrates the square of past states. Here, the nonlinearity is applied within the integral, meaning that each past state's influence is independently squared before integration. This approach may result in a different dynamic response, particularly in terms of the system's sensitivity to past values and how it aggregates those past states. Consequently, the second formulation may exhibit distinct stability characteristics and dynamic behaviors compared with the first equation, despite their structural similarity.

We consider the kernel function as the weak exponential kernel [17, 18]:

$$K(t) = e^{-\alpha t}, \qquad \alpha > 0.$$

Then, equations (1.2) and (1.3) can be rewritten as

$$\begin{aligned} &\frac{dx(t)}{dt} = 1 - \rho \left[\int_0^t e^{-\alpha(t-s)}x(s)\,ds\right]^2, \qquad t \in (0,T], \\ &x(t_0) = x_0. \end{aligned} \tag{1.4}$$

and

$$\frac{dx(t)}{dt} = 1 - \rho \int_0^t e^{-\alpha(t-s)} x^2(s)\, ds, \qquad t \in (0, T], \tag{1.5}$$
$$x(t_0) = x_0.$$

By employing the *linear chain trick* [19], these Riccati-type problems with distributed delays can be converted into systems of ordinary differential equations (ODEs), making it easier to analyze their dynamic behaviors. We define

$$y(t) = \int_0^t e^{-\alpha(t-s)} x(s)\, ds, \qquad z(t) = \int_0^t e^{-\alpha(t-s)} x^2(s)\, ds.$$

Differentiating $y(t)$ and $z(t)$ with respect to t and applying Leibniz's rule yields

$$\frac{d}{dt}\int_0^t e^{-\alpha(t-s)} x(s)\, ds = e^{-\alpha(t-t)} x(t) + \int_0^t \frac{\partial}{\partial t}\left(e^{-\alpha(t-s)}\right) x(s)\, ds$$
$$= x(t) - \alpha \int_0^t e^{-\alpha(t-s)} x(s)\, ds = x(t) - \alpha y(t).$$

Thus, for the exponential kernel, the reduction is exact and leads to the following ODE systems (see [19]):

$$\frac{dy(t)}{dt} = x(t) - \alpha y(t), \qquad \frac{dz(t)}{dt} = x^2(t) - \alpha z(t). \tag{1.6}$$

We then obtain the two equivalent systems of ODEs corresponding to equations (1.4) and (1.5) as follows:

$$\frac{dx(t)}{dt} = 1 - \rho y^2(t), \qquad x(0) = x_0, \tag{1.7}$$
$$\frac{dy(t)}{dt} = x(t) - \alpha y(t), \qquad y(0) = 0,$$

and

$$\frac{dx(t)}{dt} = 1 - \rho z(t), \qquad x(0) = x_0, \tag{1.8}$$
$$\frac{dz(t)}{dt} = x^2(t) - \alpha z(t), \qquad z(0) = 0.$$

The paper is organized as follows. Section 2 presents the stability analysis of both continuous and discrete-time feedback control for system (1.7). Section 3 provides the stability analysis of continuous and discrete-time feedback control for system (1.8). In Section 4, numerical results are presented to compare the two systems, including bifurcation diagrams, Lyapunov exponents, and phase portraits. Finally, Section 5 applies a chaos control method to stabilize the systems in chaotic regions.

2 Model (1.7)

2.1 Stability Analysis of Model (1.7)

In this section, we study the local stability of the continuous-time model (1.7).

The equilibrium points of this model are obtained by solving the following equations:

$$1 - \rho y^2 = 0,$$
$$x - \alpha y = 0.$$

Hence, we obtain two equilibrium points:

$$(x_1^*, y_1^*) = \left(\frac{\alpha}{\sqrt{\rho}}, \frac{1}{\sqrt{\rho}}\right), \quad (x_2^*, y_2^*) = \left(-\frac{\alpha}{\sqrt{\rho}}, -\frac{1}{\sqrt{\rho}}\right).$$

We analyze the stability of (1.7) by linearizing the system around each equilibrium point. This process involves approximating the nonlinear system with a linear one in the vicinity of the equilibrium points. The stability behavior is determined by examining the eigenvalues of the Jacobian matrix.

The trace–determinant method [20, 21] provides a simple yet effective approach for determining the stability of continuous dynamical systems, as stated in Lemma 2.1.

The Jacobian matrix of system (1.7) is given by:

$$J(x^*, y^*) = \begin{bmatrix} 0 & -2\rho y^* \\ 1 & -\alpha \end{bmatrix}. \tag{2.1}$$

The characteristic equation associated with (2.1) has a trace $\tau = -\alpha$ and a determinant $d = 2\rho y^*$. The eigenvalues are given by:

$$\lambda_{1,2} = \frac{1}{2}\left(\tau \pm \sqrt{\Delta}\right), \quad \text{where } \Delta = \tau^2 - 4d.$$

Lemma 2.1 ([22]). *Let (x^*, y^*) be a fixed point of a two-dimensional system. Then:*

*(i) If $\Delta > 0$, $d > 0$, and $\tau < 0$, the fixed point is a **stable node**.*

*(ii) If $\Delta > 0$, $d > 0$, and $\tau > 0$, the fixed point is an **unstable node**.*

*(iii) If $\Delta < 0$, $d > 0$, and $\tau < 0$, the fixed point is a **stable spiral**.*

*(iv) If $\Delta < 0$, $d > 0$, and $\tau > 0$, the fixed point is an **unstable spiral**.*

Proposition 2.2 (Stability of System (1.7)). *The stability of the equilibrium points of system (1.7) can be characterized as follows:*

*(i) If $\alpha^2 < 8\sqrt{\rho}$, the eigenvalues corresponding to the first equilibrium point are complex conjugates with negative real parts, indicating that it is a **stable spiral (focus)**.*

*(ii) If $\alpha^2 > 8\sqrt{\rho}$, the eigenvalues are distinct and real negative, implying that the first equilibrium point is a **stable node**.*

*(iii) The second equilibrium point (x_2^*, y_2^*) is a **saddle point**, and therefore **unstable**.*

Figures 1 and 2 illustrate the system's behavior. Figure 1 shows the phase trajectories, which visualize the flow of trajectories in the state space and provide insight into the system's dynamic behavior. Figure 2 highlights the stability region, illustrating how trajectories converge toward equilibrium points, typically indicating stable node or spiral behavior.

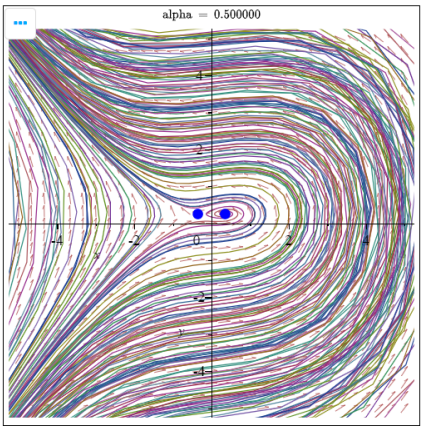

Figure 1. Phase trajectories of system (1.7).

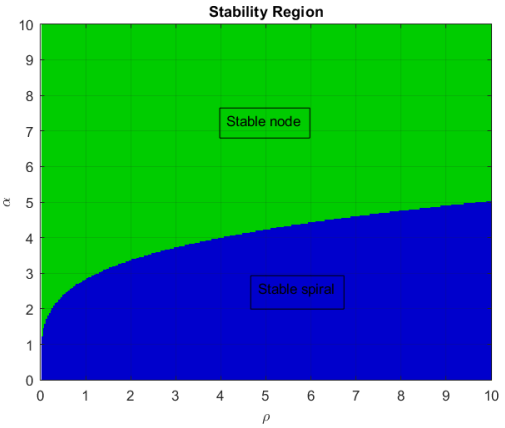

Figure 2. Stability region of system (1.7).

2.2 Discrete-Time Version of System (1.7)

In this section, we employ the method of piecewise constant arguments [15, 23, 24] to discretize system (1.7) as follows:

$$\begin{aligned} x_{n+1} &= x_n + r(1 - \rho y_n^2), \\ y_{n+1} &= y_n + r(x_n - \alpha y_n), \end{aligned} \tag{2.2}$$

where $\alpha, \rho > 0$ and r is the discretization step.

We now analyze the stability of the fixed points of the discrete system. The Jacobian matrix of system (2.2) is given by:

$$J(x^*, y^*) = \begin{bmatrix} 1 & -2r\rho y^* \\ r & 1 - \alpha r \end{bmatrix}. \tag{2.3}$$

The characteristic equation of the Jacobian matrix can be expressed as:

$$F(\lambda) = |J - \lambda I| = \lambda^2 + P\lambda + Q = 0, \tag{2.4}$$

where

$$P = -\text{tr}(J) = \alpha r - 2, \qquad Q = \det(J) = (1 - \alpha r) + 2\rho r^2 y^*.$$

To determine the local stability, we analyze the modulus of the eigenvalues of (2.4). The following lemma provides the relationships between the coefficients and the roots of a quadratic equation.

Lemma 2.3 ([25, 26]). *Let $F(\lambda) = \lambda^2 + P\lambda + Q = 0$. Suppose that $F(1) > 0$ and that $\lambda_{1,2}$ are the roots of $F(\lambda) = 0$. Then:*

- *$|\lambda_1| < 1$ and $|\lambda_2| < 1$ if and only if $F(-1) > 0$ and $Q < 1$.*
- *One root inside and one outside the unit circle ($|\lambda_1| > 1$, $|\lambda_2| < 1$ or vice versa) if and only if $F(-1) < 0$.*
- *$|\lambda_1| > 1$ and $|\lambda_2| > 1$ if and only if $F(-1) > 0$ and $Q > 1$.*
- *$\lambda_1 = -1$ and $\lambda_2 \neq 1$ if and only if $F(-1) = 0$ and $P \neq 0, 2$.*
- *λ_1 and λ_2 are complex and $|\lambda_1| = |\lambda_2| = 1$ if and only if $P^2 - 4Q < 0$ and $Q = 1$.*

At the positive fixed point

$$(x_+^*, y_+^*) = \left(\frac{\alpha}{\sqrt{\rho}}, \frac{1}{\sqrt{\rho}} \right),$$

the Jacobian matrix becomes:

$$J(x^*, y^*) = \begin{bmatrix} 1 & -2r\sqrt{\rho} \\ r & 1 - \alpha r \end{bmatrix}. \tag{2.5}$$

The corresponding characteristic equation is:

$$\lambda^2 - (-2 + r\alpha)\lambda + (1 - r\alpha + 2r^2\sqrt{\rho}) = 0, \tag{2.6}$$

with

$$P = -2 + r\alpha, \qquad Q = 1 - r\alpha + 2r^2\sqrt{\rho}.$$

Proposition 2.4 (Stability of the Discrete System). *The fixed point of system (2.2) exhibits the following stability behavior:*

*(i) The positive equilibrium (x_+^*, y_+^*) is a **sink (asymptotically stable)** if*

$$2r\sqrt{\rho} < \alpha < \frac{2 + r^2\sqrt{\rho}}{r}.$$

*(ii) It is a **source** if*

$$\alpha > \max\left(2r\sqrt{\rho}, \frac{2+r^2\sqrt{\rho}}{r}\right).$$

*(iii) It is a **saddle point** if*

$$\alpha > \frac{2+r^2\sqrt{\rho}}{r}.$$

*(iv) It is **non-hyperbolic** if any of the following conditions hold:*

- $\alpha > 8\sqrt{\rho}$ *and* $\alpha = \frac{2+r^2\sqrt{\rho}}{r}$, *where* $\alpha \neq \frac{2}{r}, \frac{4}{r}$.
- $\alpha < 8\sqrt{\rho}$ *and* $\alpha = 2r\sqrt{\rho}$.

(v) The negative fixed point (x_-^*, y_-^*) *is **unstable**.*

3 The model (1.8)

3.1 The fixed point and stability analysis

In this section, we examine the local stability of the continuous-time model (1.8). The equilibrium points for this model are determined by solving the following equations:

$$1 - \rho z = 0,$$
$$x^2 - \alpha z = 0.$$

Hence, the system (1.8) possesses two equilibrium points given by

$$(x_1^*, z_1^*) = \left(\sqrt{\frac{\alpha}{\rho}}, \frac{1}{\rho}\right), \quad (x_2^*, z_2^*) = \left(-\sqrt{\frac{\alpha}{\rho}}, \frac{1}{\rho}\right).$$

To analyze the local stability, we linearize the system around each equilibrium point. The Jacobian matrix of system (1.8) is given by

$$J(x^*, z^*) = \begin{bmatrix} 0 & -\rho \\ 2x^* & -\alpha \end{bmatrix}. \tag{3.1}$$

The characteristic polynomial of (3.1) has trace $\tau = -\alpha$ and determinant $d = 2\rho x^*$. Using Lemma (2.1), the local stability can be characterized as follows:

Proposition 3.1 (Stability of the system (1.8)). *(i) If* $\alpha^2 < 8\sqrt{\rho\alpha}$, *the eigenvalues associated with the first equilibrium point are complex conjugates with negative real parts, indicating that it is a **stable spiral (focus)**.*

(ii) If $\alpha^2 > 8\sqrt{\rho\alpha}$, *the eigenvalues are distinct and real negative, implying that the first equilibrium point is a **stable node**.*

(iii) The second equilibrium point (x_2^*, z_2^*) *is a **saddle point**, hence unstable.*

The phase diagram illustrates the trajectories in the x–z plane. Figure (3) shows that the precise dynamics can be visualized effectively through the phase diagram, which helps in understanding the flow of trajectories in the system's state space. Figure (4) illustrates the stability region of the system, where trajectories converge toward an equilibrium point, typically indicating a stable node or a stable spiral.

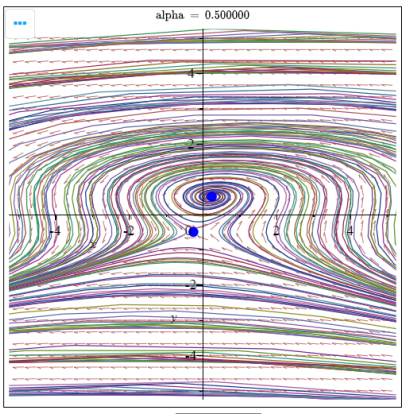

Figure 3. Phase trajectories of system (1.8).

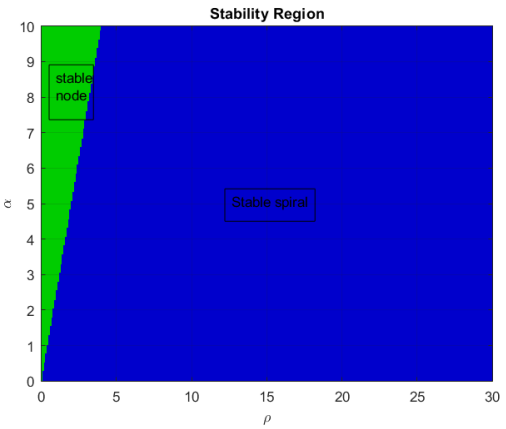

Figure 4. Stability region of system (1.8).

3.2 The discrete-time system of (1.8)

We now apply the *piecewise constant argument* to discretize the system (1.8), yielding

$$\begin{aligned} x_{n+1} &= x_n + r(1 - \rho z_n), \\ z_{n+1} &= z_n + r(x_n^2 - \alpha z_n). \end{aligned} \tag{3.2}$$

The Jacobian matrix of the discrete-time system (3.2) is given by

$$J(x^*, z^*) = \begin{bmatrix} 1 & -r\rho \\ 2rx^* & 1 - \alpha r \end{bmatrix}. \tag{3.3}$$

Lemma (2.3) provides the criteria for determining the local stability of (3.2), where

$$P = \alpha r - 2, \qquad Q = (1 - \alpha r) + 2\rho r^2 x^*.$$

Proposition 3.2 (Stability of the discrete system (3.2)). *The fixed point* (x_1^*, z_1^*) *of system (3.2) exhibits the following behavior:*

(i) (x_1^*, z_1^*) *is a* ***sink (asymptotically stable)*** *if*

$$\frac{\alpha r - 2}{r^2\sqrt{\alpha}} < \sqrt{\rho} < \frac{\sqrt{\alpha}}{2r}.$$

(ii) It is a ***source (unstable)*** *if*

$$\sqrt{\rho} > \max\left(\frac{\alpha r - 2}{r^2\sqrt{\alpha}}, \frac{\sqrt{\alpha}}{2r}\right).$$

(iii) It is a ***saddle point*** *if*

$$0 < \sqrt{\rho} < \frac{\alpha r - 2}{r^2\sqrt{\alpha}}.$$

(iv) It is ***non-hyperbolic*** *if* $\rho > \frac{\alpha^3}{64}$ *and* $\alpha = 4r^2\rho$.

(v) The second equilibrium point (x_2^*, z_2^*) *is* ***unstable***.

4 Numerical Simulations and Dynamic Analysis

In this section, we present numerical simulations to illustrate the bifurcation diagrams, phase portraits, and Lyapunov exponents of systems (2.2) and (3.2). These simulations confirm the analytical results obtained earlier and reveal additional complex dynamical behaviors exhibited by both systems.

It is well known that the *maximum Lyapunov exponent* (MLE) serves as a key indicator of chaos, quantifying the exponential divergence of initially close trajectories in the state space. A positive MLE implies chaotic behavior, while a negative MLE indicates asymptotic stability. We take the initial condition $(x_0, y_0) = (0.1, 0.1)$ and vary the parameter r, which acts as the bifurcation parameter, while keeping the other parameters fixed.

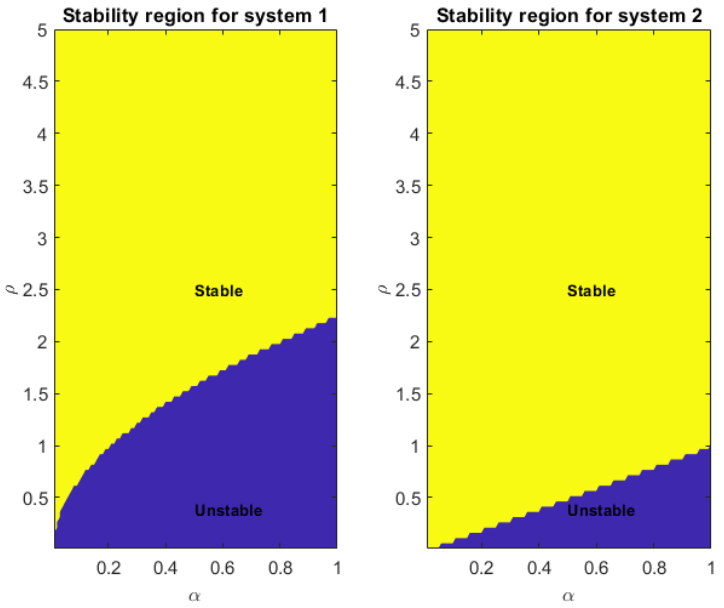

Figure 5. Stability for $r = 0.1$.

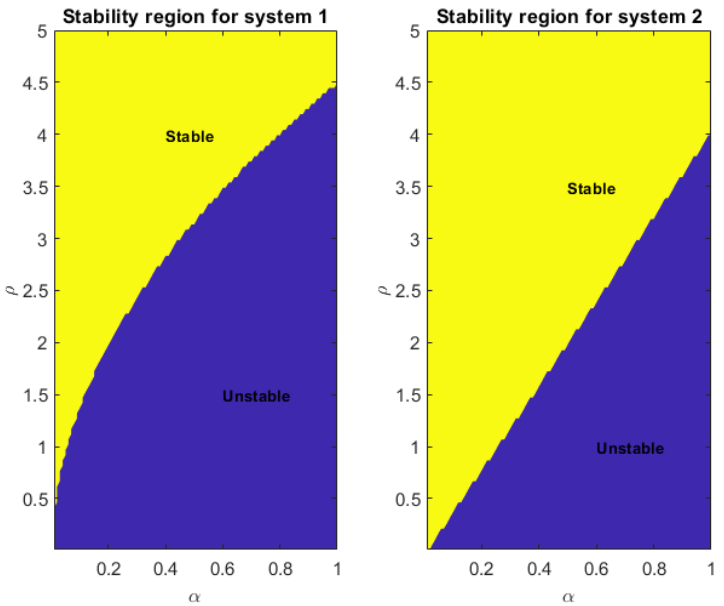

Figure 6. Stability for $r = 0.2$.

The stability regions of the two systems, as shown in Figures 5 and 6, illustrate the influence of the parameter r on the dynamic behavior of the system.

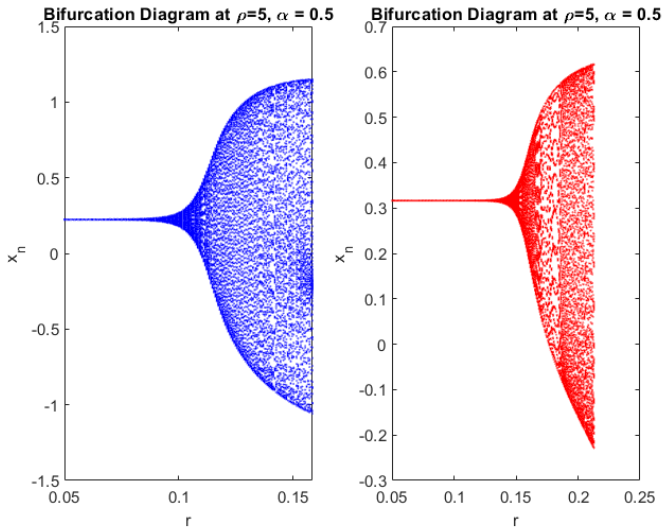

Figure 7. Bifurcation diagram of the two systems (2.2) and (3.2), showing the qualitative changes in their dynamic behavior as the parameter r varies, with fixed parameters $\alpha = 0.5$ and $\rho = 5$.

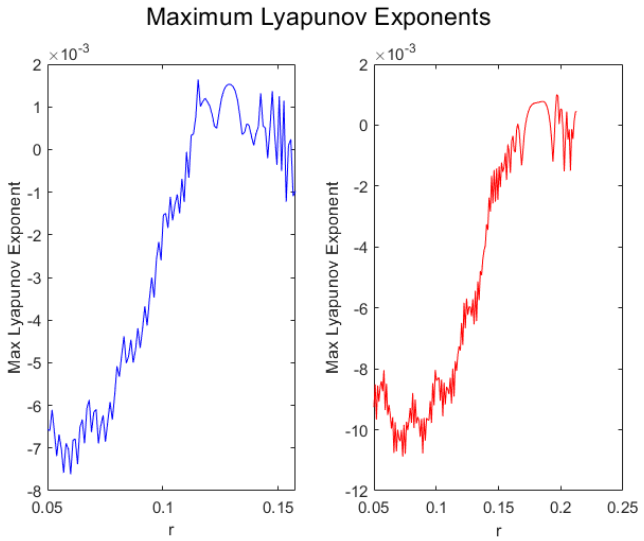

Figure 8. Lyapunov exponent diagram illustrating the transition between stable and chaotic regimes of the two systems (2.2) and (3.2) as r changes, for fixed parameters $\alpha = 0.5$ and $\rho = 5$.

Figures 7–10 present the bifurcation diagrams and the corresponding maximal Lyapunov exponents (MLEs) for both systems. In these plots, the blue curves correspond to system 2.2, whereas the red curves represent system 3.2. The results clearly demonstrate distinct bifurcation patterns between the two systems, indicating different pathways to instability and chaos. In both cases, the bifurcations are identified as being of the Neimark–Sacker type.

As illustrated in Figure 7, the bifurcation diagram of system 2.2 shows a loss of stability at approximately $r = 0.10$ and $r = 0.15$, whereas system 3.2 (Figure 9) remains stable until about $r = 0.39$ and $r = 0.68$, respectively. This comparison demonstrates that system 3.2 preserves

stability over a wider range of the control parameter r before transitioning to chaotic behavior

The maximal Lyapunov exponents were calculated numerically using the Benettin–Wolf algorithm [27], which integrates the system together with its variational equations, periodically re-orthonormalizing the tangent vectors. A positive MLE signifies chaotic dynamics, whereas a negative value indicates stable motion. The computed Lyapunov exponent plots (Figures 8 and 10) confirm that chaos emerges more rapidly in System 1, with divergence observed near $r = 0.11$ and $r = 0.16$. In contrast, System 2 exhibits a delayed onset of chaos, occurring around $r = 0.7$ and $r = 0.54$, respectively.

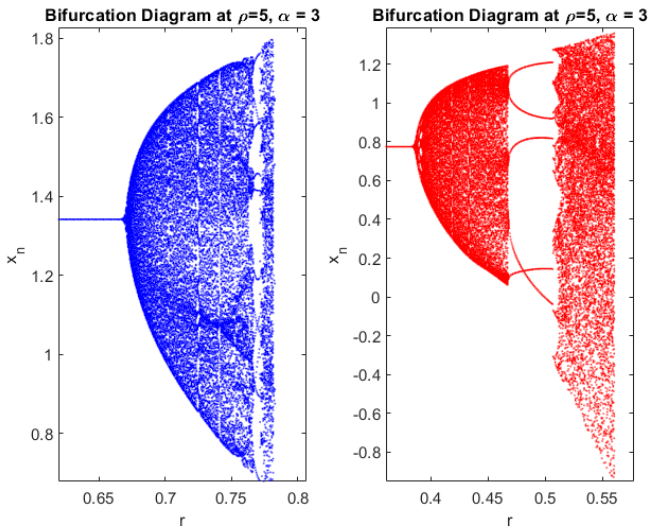

Figure 9. Bifurcation diagram of the two systems (2.2) and (3.2), showing the qualitative changes in their dynamic behavior as the parameter r varies, with fixed parameters $\alpha = 3$ and $\rho = 5$.

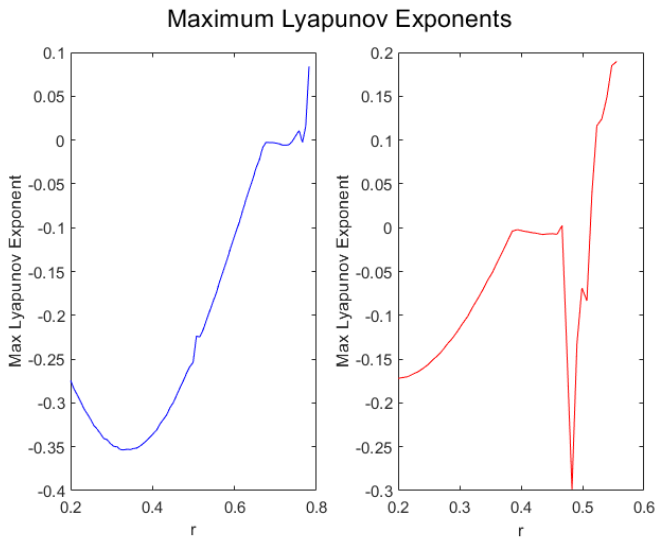

Figure 10. Lyapunov exponent diagram illustrating the transition between stable and chaotic regimes of the two systems (2.2) and (3.2) as r changes, for fixed parameters $\alpha = 3$ and $\rho = 5$.

The phase portraits in Figures 11–15 are plotted from the initial condition $(0.1, 0.1)$ for different parameter values. For $r = 0.1$, $\rho = 5$, and $\alpha = 0.5$, both systems exhibit stability. For system

2.2, the eigenvalues are $0.9750 \pm 0.1761i$, giving $|\lambda_{1,2}| = 0.9908 < 1$, which confirms stability. Similarly, for system 3.2, the eigenvalues are $0.9750 \pm 0.2100i$, with $|\lambda_{1,2}| = 0.9974 < 1$, as shown in Figure 11. The complex eigenvalues imply that the equilibrium points are stable foci, exhibiting spiral trajectories converging to equilibrium.

As α increases, both systems become more rapidly stable, which is reflected in faster trajectory convergence. The higher α value strengthens the damping effect, reducing transient oscillations and accelerating the decay toward equilibrium, as shown in Figure 12.

Figure 13 illustrates that system 2.2 exhibits periodic oscillations for $r = 0.1$, $\alpha = 0.5$, and $\rho = 12$, while system 3.2 takes longer to stabilize under the same conditions. Furthermore, Figures 14 and 15 confirm that increasing α enhances the stability of both systems by reducing the time to reach equilibrium.

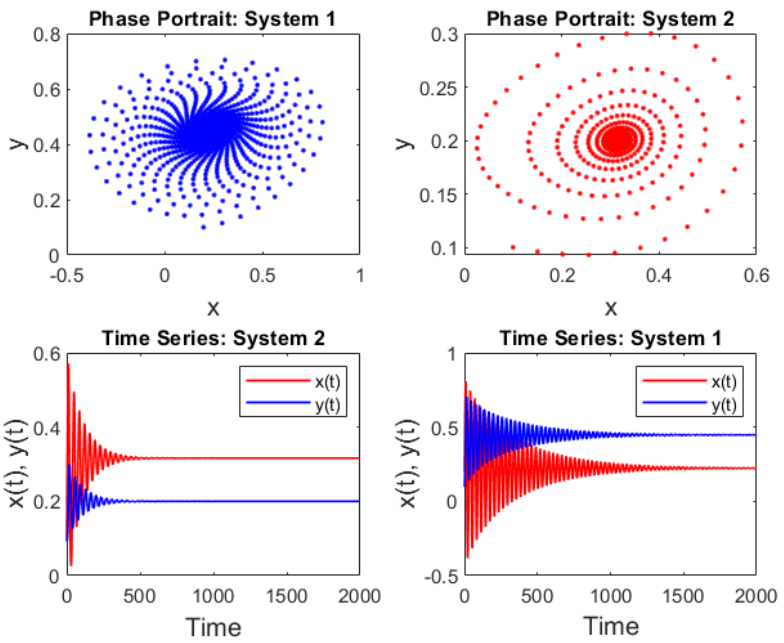

Figure 11. Phase portrait for $r = 0.1$, $\rho = 5$, $\alpha = 0.5$.

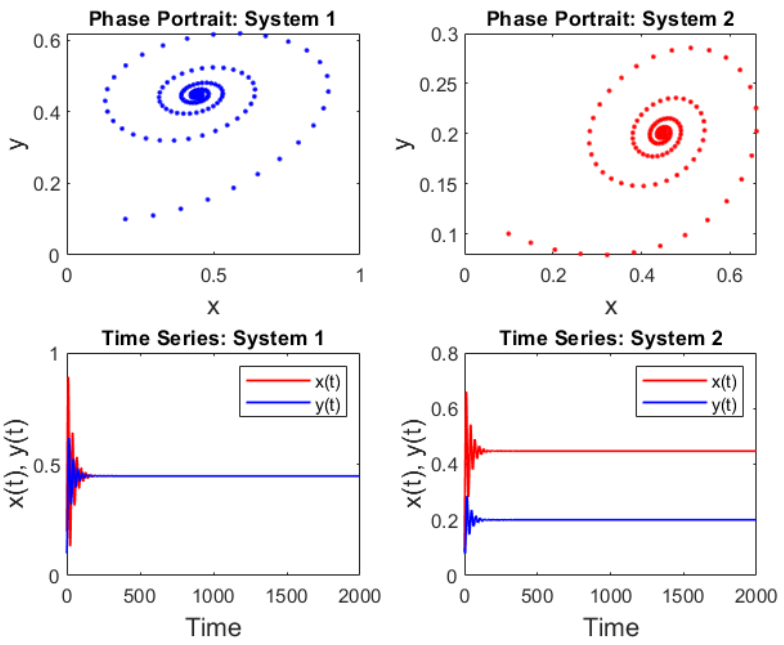

Figure 12. Phase portrait for $r = 0.1$, $\rho = 5$, $\alpha = 1$.

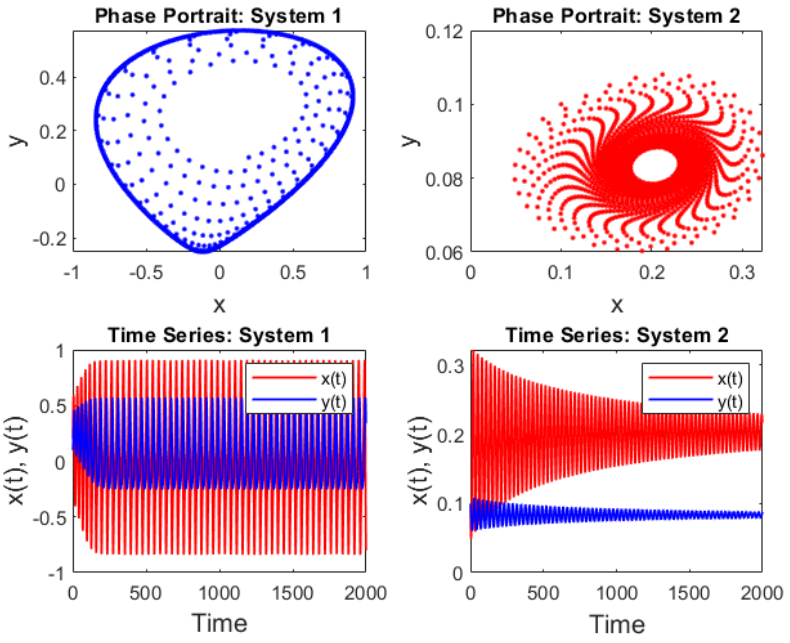

Figure 13. Phase portrait for $r = 0.1$, $\rho = 12$, $\alpha = 0.5$.

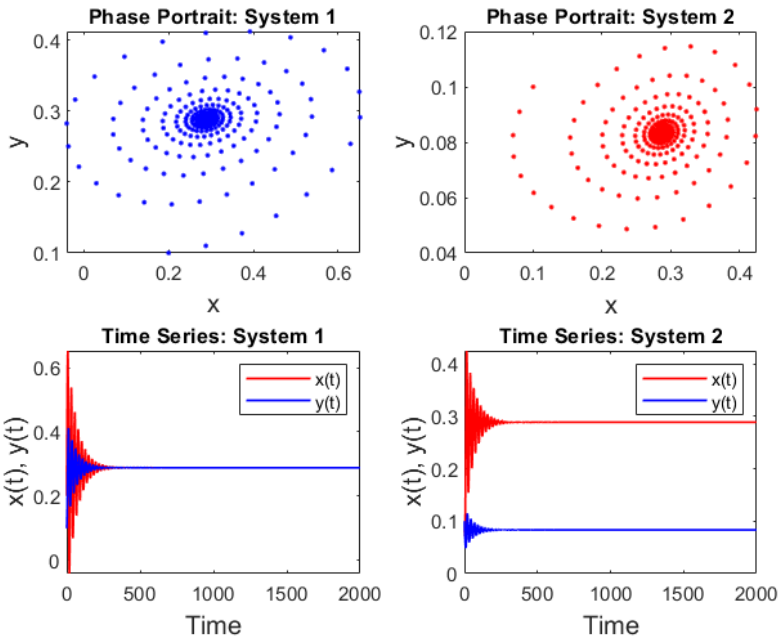

Figure 14. Phase portrait for $r = 0.1$, $\rho = 12$, $\alpha = 0.9$.

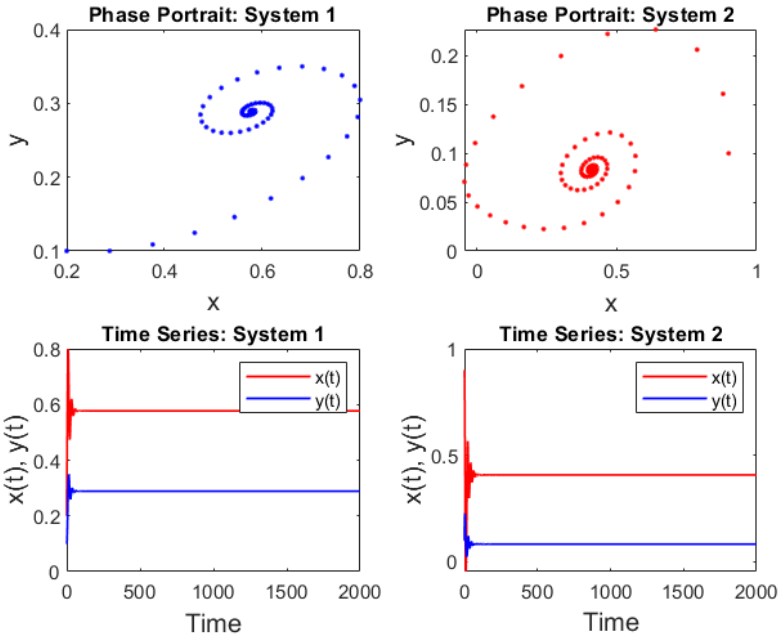

Figure 15. Phase portrait for $r = 0.1$, $\rho = 12$, $\alpha = 2$.

5 Chaos Control

In this section, we discuss the chaos control method [26, 28, 29] applied to the feedback-controlled systems (2.2) and (3.2) to stabilize an unstable fixed point.

5.1 Chaos control for system (2.2)

Consider the following controlled form of system (2.2):

$$\begin{aligned} x_{n+1} &= x_n + r(1 - \rho y_n^2) + u_n, \\ y_{n+1} &= y_n + r(x_n - \alpha y_n), \end{aligned} \tag{5.1}$$

where $u_n = -k_1(x_n - x^*) - k_2(y_n - y^*)$ represents the control force. The Jacobian matrix of the controlled system (5.1) at the fixed point (x^*, y^*) is

$$J(x^*, y^*) = \begin{bmatrix} 1 - k_1 & -2r\rho y^* - k_2 \\ r & 1 - \alpha r \end{bmatrix} = \begin{bmatrix} 1 - k_1 & -2r\sqrt{\rho} - k_2 \\ r & 1 - \alpha r \end{bmatrix}. \tag{5.2}$$

The trace and determinant of the Jacobian are given by

$$\mathrm{Tr}(J) = \lambda_1 + \lambda_2 = 2 - r\alpha - k_1, \tag{5.3}$$

$$\det(J) = \lambda_1\lambda_2 = (1 - k_1)(1 - \alpha r) + 2r^2\sqrt{\rho} + rk_2. \tag{5.4}$$

The conditions $\lambda_1 = \pm 1$ and $\lambda_1\lambda_2 = 1$ define the lines of marginal stability, which ensure that the modulus of the eigenvalues satisfies $|\lambda_{1,2}| < 1$. These lines are given by:

$$l_1 : \quad (1 - \alpha r)k_1 - rk_2 = 2r^2\sqrt{\rho} - \alpha r, \tag{5.5}$$

$$l_2 : \quad (\alpha r)k_1 - rk_2 = 1 + 2r^2\sqrt{\rho}, \tag{5.6}$$

$$l_3 : \quad (2 - \alpha r)k_1 - rk_2 = 4 - 2\alpha r + 2r^2\sqrt{\rho}. \tag{5.7}$$

The stable eigenvalues lie in the triangular region bounded by l_1, l_2, and l_3 in Figure 16.

To demonstrate the effect of state-feedback control, we performed numerical simulations with parameters $\alpha = 0.5$, $r = 0.1$, $\rho = 12$, and feedback gains $k_1 = 2$, $k_2 = 5$. The initial condition is $(x_0, y_0) = (0.1, 0.1)$. Figures 17 and 18 shows how the chaotic trajectory is stabilized to the fixed point $(0.1443, 0.2887)$.

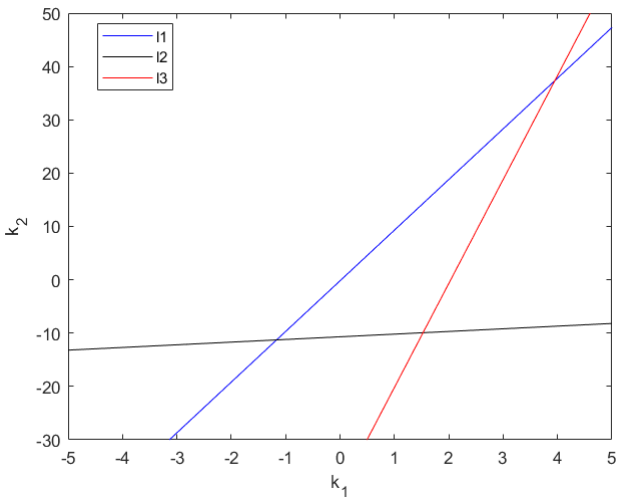

Figure 16. Triangular region for stabilizing the fixed point with $\alpha = 0.5$, $r = 0.1$, $\rho = 12$.

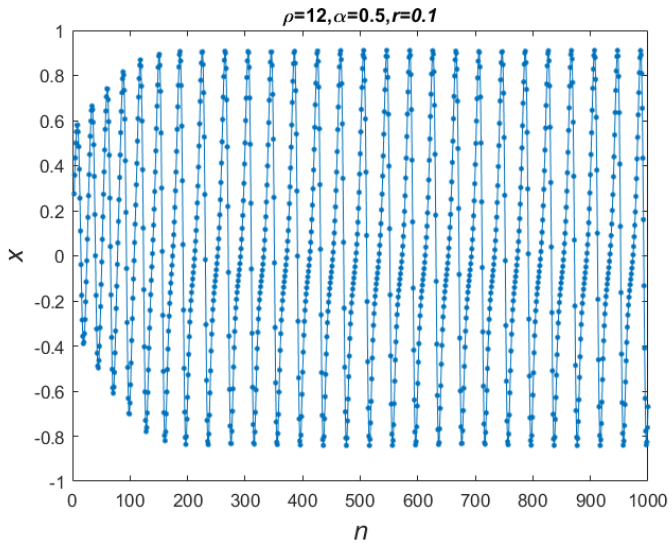

Figure 17. Time series of System (2.2) before applying chaos control, showing irregular oscillatory behavior corresponding to chaotic dynamics. Parameters: $\alpha = 0.5$, $r = 0.1$, and $\rho = 12$.

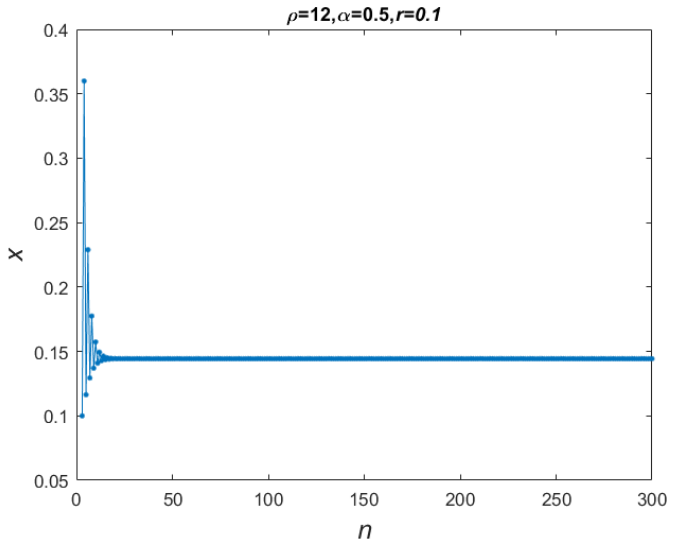

Figure 18. Time series of System (2.2) after applying chaos control, illustrating the suppression of chaotic oscillations and the emergence of stable periodic motion. Parameters: $\alpha = 0.5$, $r = 0.1$, and $\rho = 12$.

5.2 Chaos control for system (3.2)

Similarly, the controlled form of system (3.2) is

$$\begin{aligned} x_{n+1} &= x_n + r(1 - \rho y_n) + u_n, \\ y_{n+1} &= y_n + r(x_n^2 - \alpha y_n), \end{aligned} \tag{5.8}$$

where $u_n = -k_1(x_n - x^*) - k_2(y_n - y^*)$. The Jacobian matrix at (x^*, y^*) is

$$J(x^*, y^*) = \begin{bmatrix} 1 - k_1 & -\rho r - k_2 \\ 2rx^* & 1 - \alpha r \end{bmatrix}. \tag{5.9}$$

The marginal stability lines are

$$l_1: \quad (1-\alpha r)k_1 - 2r\sqrt{\frac{\alpha}{\rho}}k_2 = 2r^2\sqrt{\alpha\rho} - \alpha r, \tag{5.10}$$

$$l_2: \quad (\alpha r)k_1 - 2r\sqrt{\frac{\alpha}{\rho}}k_2 = -2r^2\sqrt{\alpha\rho}, \tag{5.11}$$

$$l_3: \quad (2-\alpha r)k_1 - 2r\sqrt{\frac{\alpha}{\rho}}k_2 = 4 - 2\alpha r + 2r^2\sqrt{\alpha\rho}. \tag{5.12}$$

The stable eigenvalues lie in the triangular region bounded by l_1, l_2, and l_3 as shown in Figure 19 for fixed parameters $\rho = 5$, $\alpha = 0.5$, $r = 0.17$.

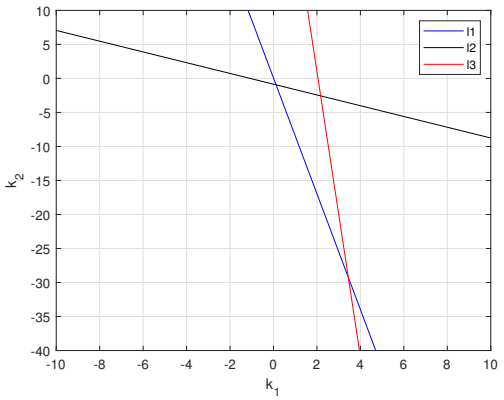

Figure 19. Triangular region for stabilizing the fixed point with $\alpha = 0.5$, $r = 0.17$, $\rho = 5$.

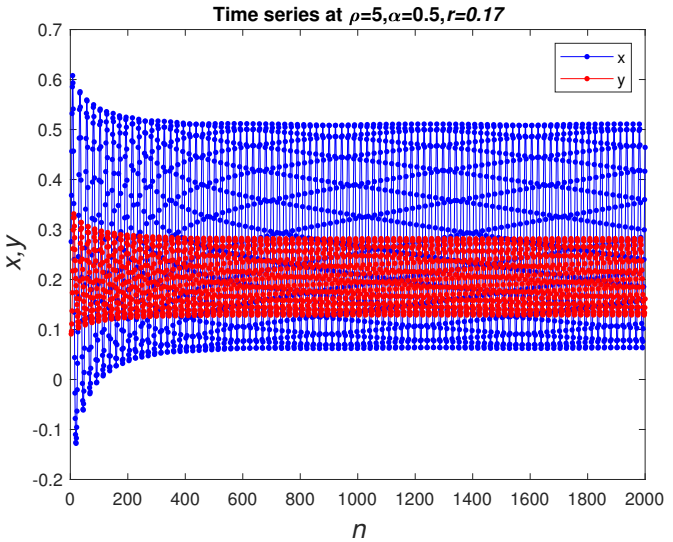

Figure 20. Time series before chaos control of the system (3.2).

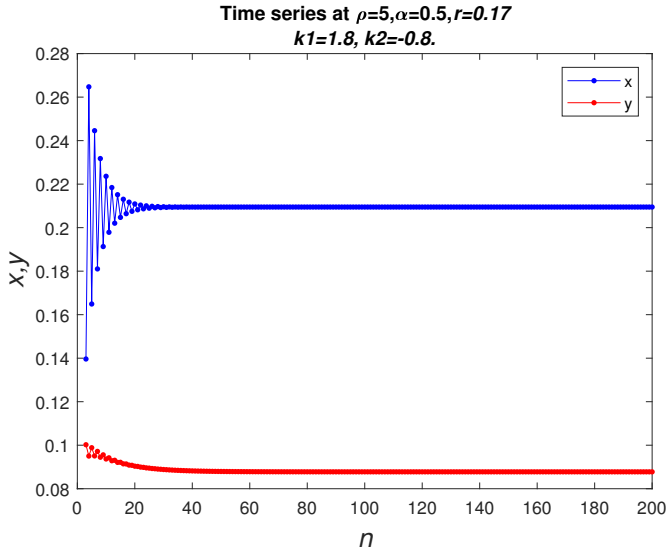

Figure 21. Time series after chaos control of the system (3.2) with $k_1 = 1.8$, $k_2 = -0.8$.

Figure 20 illustrates the chaotic behavior before applying the control technique, showing unpredictable and erratic oscillations characteristic of chaos. After implementing the feedback control, as shown in Figure 21, the system converges to a stable fixed point or a periodic orbit. This demonstrates the effectiveness of the chaos control method in transforming chaotic dynamics into predictable and stable behavior.

Applications of the Ricatti Problem

The studied Riccati-type system with distributed delay has several important real-world applications. Such models arise naturally in various biological and engineering contexts where feedback mechanisms and memory effects play a crucial role. For instance, in biological systems, the model can describe the glucose–insulin regulatory process, in which the insulin action exhibits a delayed response to blood glucose levels distributed over time. Similar formulations are also useful in modeling population dynamics with hereditary effects, physiological control systems, and feedback control processes in engineering. These examples demonstrate the practical relevance and applicability of the proposed theoretical analysis to real-world delayed dynamical phenomena.

5.3 Future Work

In future work, I plan to study the detailed dynamics of this glucose-insulin Riccati-type system, including numerical simulations, bifurcation analysis, and the design of optimal feedback controllers to maintain stable glucose levels under varying physiological conditions. Also we extend the current analysis of distributed-delay Riccati-type systems in several directions. One important extension is the application of distributed-delay in neural network dynamics, particularly by considering different kernel functions to represent various memory and learning effects.Moreover, incorporating fractional-order derivatives could enhance the modeling of complex temporal behaviors in such systems. Another potential direction involves exploring adaptive control, synchronization, and bifurcation phenomena in coupled or higher-dimensional Riccati systems. These developments will broaden the applicability of the proposed framework and provide deeper insights into the interplay between delay, nonlinearity, and stability in real-world systems.

6 Conclusion

In this paper, we have explored and compared the stability properties of two types of Riccati equations in both discrete and continuous time domains. Our analysis reveals that the parameter α plays a crucial role in determining the stability of distributed delay systems. Numerical simulations demonstrate that varying α significantly affects the stability landscape, with higher values of α leading to improved stability and quicker convergence to equilibrium. The maximal Lyapunov exponent and phase portraits provide additional clarity, showing how the systems transition from stable to chaotic behavior as parameters are varied. Moreover, we applied the method of chaos control to further refine the system's dynamics. By introducing chaos control techniques, we successfully stabilized the chaotic regions identified in the simulations, restoring predictable and stable behavior even in regions prone to instability. Our findings highlight the effectiveness of α in controlling system dynamics and offer valuable insights into the behavior of Riccati systems under different conditions. This study not only contributes to the theoretical understanding of Riccati equations but also offers practical implications for designing stable dynamical systems.

Statements and Declarations

The author declares that he has no known competing financial interests or personal relationships that could have appeared to influence the work reported in this paper.

References

[1] Masani, P. R. (2012). *Norbert Wiener 1894–1964*. Birkhäuser.

[2] Banerjee, M. & Zhang, L. (2016). Time delay can enhance spatio-temporal chaos in a prey–predator model. *Ecological Complexity*, 27, 17–28.

[3] Bajiya, V. P., Tripathi, J. P., Kakkar, V., Wang, J. & Sun, G. (2021). Global dynamics of a multi-group SEIR epidemic model with infection age. *Chinese Annals of Mathematics B*, 42(6), 833–860.

[4] Torbensen, K., Rossi, F., Ristori, S. & Abou-Hassan, A. (2017). Chemical communication and dynamics of droplet emulsions in networks of Belousov–Zhabotinsky micro-oscillators. *Lab on a Chip*, 17(7), 1179–1189.

[5] Chembo, Y. K., Brunner, D., Jacquot, M. & Larger, L. (2019). Optoelectronic oscillators with time-delayed feedback. *Reviews of Modern Physics*, 91(3), 035006.

[6] Larger, L. (2013). Complexity in electro-optic delay dynamics: modelling, design and applications. *Philosophical Transactions of the Royal Society A*, 371(1999), 20120464.

[7] Richard, J.-P. (2003). Time-delay systems: an overview of recent advances and open problems. *Automatica*, 39(10), 1667–1694.

[8] Bianca, C., Ferrara, M. & Guerrini, L. (2013). The time delays' effects on economic growth model. *Abstract and Applied Analysis*, 2013(1), 901014.

[9] Bischi, G.-I., Chiarella, C., Kopel, M. & Szidarovszky, F. (2010). *Nonlinear oligopolies*. Springer.

[10] Smith, H. (2011). Distributed delay equations and the linear chain trick. In *An introduction to delay differential equations with applications to the life sciences* (pp. 119–130). Springer.

[11] Zhang, C. H., Yan, X. P. & Cui, G. H. (2010). Hopf bifurcations in a predator–prey system with discrete and distributed delay. *Nonlinear Analysis: Real World Applications*, 11(5), 4141–4153.

[12] Guerrini, L., Pecora, N. & Sodini, M. (2018). Effects of fixed and continuously distributed delays in a monopoly model. *Decisions in Economics and Finance*, 41, 239–257.

[13] Rihan, F. A., Udhayakumar, K., Sottocornola, N., Anwar, M.-N. & Khaliq, A. Q. M. (2023). Stability and bifurcation analysis of the Caputo fractional-order asymptomatic COVID-19 model with multiple time-delays. *Int. J. Bifurcation and Chaos*, 33(2), 2350022.

[14] Rihan, F. A., Hashish, A., Al-Maskari, F., Hussein, M. S., Ahmed, E., Riaz, M. B. & Yafia, R. (2016). Dynamics of tumor-immune system with fractional-order. *Journal of Tumor Research*, 2(1), 109–115.

[15] El-Sayed, A. M. A. & Salman, S. M. (2013). On a discretization process of fractional-order Riccati differential equation. *J. Fract. Calc. Appl.*, 4(2), 251–259.

[16] A. M. A. El-Sayed, S. M. Salman, and M. A. Saad, "On some dynamic properties of a distributed delay model," *Bulletin of Mathematical Analysis and Applications*, vol. 16, no. 4, pp. 1821–1291, 2024.

[17] Wu, J., Zhan, X. S., Zhang, X. H. & Gao, H. L. (2012). Stability and Hopf bifurcation on a numerical discretization of the distributed delay equation. *Chinese Physics Letters*, 29(5), 050203.

[18] Shi, X., Zhou, X. & Song, X. (2010). Dynamical behavior for an eco-epidemiological model with discrete and distributed delay. *Journal of Applied Mathematics and Computing*, 33(1-2), 305–325.

[19] Smith, H. L. (2011). *An introduction to delay differential equations with applications to the life sciences*. Springer New York.

[20] D. Lathrop, *Nonlinear Dynamics and Chaos: With Applications to Physics, Biology, Chemistry, and Engineering*, American Institute of Physics, 2015.

[21] Hirsch, M. W., Smale, S. & Devaney, R. L. (2012). *Differential equations, dynamical systems, and an introduction to chaos*. Academic Press.

[22] Strogatz, S. H. (2001). *Nonlinear Dynamics and Chaos*. Westview Press.

[23] El-Sayed, A. M. A. & Salman, S. M. (2013). Chaos and bifurcation of the logistic discontinuous dynamical systems with piecewise constant arguments. *Malaya Journal of Matematik*, 1(3), 14–20.

[24] Akhmet, M. U. (2008). Stability of differential equations with piecewise constant arguments of generalized type. *Nonlinear Analysis*, 68(4), 794–803.

[25] Kuznetsov, Y. A. (1998). *Elements of applied bifurcation theory*. Springer.

[26] He, Z. & Lai, X. (2011). Bifurcation and chaotic behavior of a discrete-time predator-prey system. *Nonlinear Analysis: Real World Applications*, 12(1), 403–417.

[27] Wolf, A., Swift, J. B., Swinney, H. L. & Vastano, J. A. (1985). Determining Lyapunov exponents from a time series. *Physica D*, 16(3), 285–317.

[28] Lynch, S. (2007). *Dynamical systems with applications using Mathematica*. Springer.

[29] Chen, G. & Dong, X. (1998). *From chaos to order: methodologies, perspectives and applications*. World Scientific.

Author information

A.M.A. El-Sayed, Department of Mathematics, Faculty of Science, Alexandria University., Egypt.
E-mail: amasayed@alexu.edu.eg

S.M. Salman, Department of Mathematics, Faculty of Education, Alexandria University, Egypt.
E-mail: samastars9@gmail.com

M.A. Saad, Faculty of Science, Alexandria University., Egypt.
E-mail: muhammed.saad@alexu.edu.eg

Received: 2025-08-30
Accepted: 2025-11-03